Response of the Global Surface Ozone Distribution to Northern Hemisphere Sea Surface Temperature Changes: Implications for Long-Range Transport

Kan Yi[1], Junfeng Liu[1], George Ban-Weiss[2], Jiachen Zhang[2], Wei Tao[1], Shu Tao[1]

[1] Laboratory for Earth Surface Processes, College of Urban and Environmental Sciences, Peking University, Beijing, China

[2] Sonny Astani Department of Civil and Environmental Engineering, University of Southern California, U.S.A.

Correspondence to: Junfeng Liu (E-mail: jfliu@pku.edu.cn)

Abstract

The response of surface ozone (O_3) concentrations to basin-scale warming and cooling of Northern Hemisphere oceans is investigated using the Community Earth System Model (CESM). Idealized, spatially uniform sea surface temperature (SST) anomalies of +/- 1 °C are individually superimposed onto the North Pacific, North Atlantic, and North Indian Oceans. Our simulations suggest large seasonal and regional variability of surface O_3 in response to SST anomalies, especially in the boreal summer. The responses of surface O_3 associated with basin-scale SST warming and cooling have similar magnitude but are opposite in sign. Increasing the SST by 1 °C in one of the oceans generally decreases the surface O_3 concentrations from 1 to 5 ppbv. With fixed emissions, SST increases in a specific ocean basin in the Northern Hemisphere tend to increase the summertime surface O_3 concentrations over upwind regions, accompanied by a widespread reduction over downwind continents. We implement the integrated process rate (IPR) analysis in CESM and find that meteorological O_3 transport in response to SST changes is the key process causing surface O_3 perturbations in most

cases. During the boreal summer, basin-scale SST warming facilitates the vertical transport of O_3 to the surface over upwind regions while significantly reducing the vertical transport over downwind continents. This process, as confirmed by tagged CO-like tracers, indicates a considerable suppression of intercontinental O_3 transport due to increased tropospheric stability at lower mid-latitudes induced by SST changes. On the other hand, the responses of chemical O_3 production to regional SST warming can exert positive effects on surface O_3 levels over highly polluted continents, except South Asia, where intensified cloud loading in response to North Indian SST warming depresses both the surface air temperature and solar radiation, and thus photochemical O_3 production. Our findings indicate a robust linkage between basin-scale SST variability and continental surface O_3 pollution, which should be considered in regional air quality management.

Keywords: SST anomaly, Surface O_3, Process analysis, Transport, CESM

1. Introduction

High ground-level ozone (O_3) concentrations adversely impact human health by inducing respiratory diseases and threaten food security by lowering crop yields (Brown and Bowman, 2013;Organization, 2013;Chuwah et al., 2015). Considering the eco-toxicity of O_3, understanding the physical and chemical mechanisms that control atmospheric O_3 concentrations is of great importance. Surface O_3 is produced in the atmosphere via photochemical processing of multiple precursors including volatile organic compounds (VOCs), carbon monoxide (CO) and nitrogen oxides (NO, NO_2). These precursors originate from both natural and anthropogenic sources (Vingarzan, 2004;Simon et al., 2014;Jiang et al., 2016). In addition to local production, transport of O_3 and its precursors from upwind regions and the upper atmosphere can also influence surface O_3 abundance. Stratospheric intrusion events, which lead to vertical down-mixing of ozone-rich air, can significantly elevate surface O_3 during spring and summer

(Grewe, 2006;Lin et al., 2012b;Zhang et al., 2014). The long-range transport of O_3 and its precursors has been extensively studied, and their inter-continental impacts have been evaluated using measurements and model simulations (Parrish et al., 1993;Fehsenfeld et al., 1996;Wild and Akimoto, 2001;Creilson et al., 2003;Simmonds et al., 2004;Fiore et al., 2009;Brown-Steiner and Hess, 2011;Lin et al., 2012a;Lin et al., 2014).

Both photochemistry and dynamic transport collectively affect surface O_3 levels. Important meteorological factors that can impact both photochemistry and transport include atmospheric circulations, solar radiation, air temperature, and relative humidity. Atmospheric circulation considerably determines the timescale and pathway of O_3 transport (Bronnimann et al., 2000;Auvray and Bey, 2005;Hess and Mahowald, 2009). The efficiency of O_3 transport varies coherently with atmospheric circulations on different scales. Knowland et al. (2015) demonstrated the important role of mid-latitude storms in redistributing O_3 concentrations during springtime. The North Atlantic Oscillation (NAO) significantly affects surface and tropospheric O_3 concentrations over most of Europe by influencing the intercontinental transport of air masses (Creilson et al., 2003;Christoudias et al., 2012;Pausata et al., 2012). Lamarque and Hess (2004) indicated that the Arctic Oscillation (AO) can modulate springtime tropospheric O_3 burdens over North America. The shift in the position of the jet stream associated with climate change was found to strongly affect summertime surface O_3 variability over eastern North America (Barnes and Fiore, 2013). Increases in solar radiation and air temperature can increase the rate of the chemical production of O_3 and modulate the biogenic emissions of O_3 precursors (Guenther, 1993;Sillman and Samson, 1995;Peñuelas and Llusià, 2001), especially over highly polluted regions (Ordónez et al., 2005;Rasmussen et al., 2012;Pusede et al., 2015). Increases in humidity can enhance the chemical destruction of O_3 and shorten its atmospheric lifetime (Johnson et al., 1999;Camalier et al., 2007). Therefore, changes in meteorological conditions on various spatial and temporal scales play key roles in determining the surface O_3 distribution. Understanding the mechanisms and feedbacks of the interactions between

92 O_3 and climate has received increasing attention and will be essential for future surface
93 O_3 mitigation (Jacob and Winner, 2009;Doherty et al., 2013).
94
95 Sea surface temperature (SST) is an important indicator that characterizes the state of
96 the climate system. Its variations strongly perturb the mass and energy exchange
97 between the ocean and atmosphere (Small et al., 2008;Gulev et al., 2013), which further
98 influence atmospheric circulation, solar radiation, atmospheric temperature and specific
99 humidity (Sutton and Hodson, 2005;Frankignoul and Sennéchael, 2007;Li et al., 2008)
100 from regional to global scales (Glantz et al., 1991;Wang et al., 2000;Goswami et al.,
101 2006). Numerous studies have shown that SST changes over different oceans and at
102 different latitudes lead to significantly different meteorological sensitivities and climate
103 responses (Webster, 1981;Lau and Nath, 1994;Lau, 1997;Sutton and Hodson,
104 2007;Sabeerali et al., 2012;Ueda et al., 2015). Details on the SST-climate relationships
105 over individual oceanic regions are summarized in Kushnir et al. (2002).
106
107 SSTs are generally increasing due to the impacts of anthropogenic forcings on global
108 climate change (IPCC, 2013, Chapter 2). In addition, regional SST exhibits natural
109 periodic or irregular oscillations with timescales ranging from months to decades. The
110 El Niño/Southern Oscillation (ENSO) is the most influential natural SST variability that
111 originates in the tropical Pacific and has worldwide climate impacts (Philander,
112 1983;Wang et al., 2012). The Pacific decadal oscillation (PDO), defined by ocean
113 temperature anomalies in the northeast and tropical Pacific Ocean, is another long-lived,
114 El Niño-like pattern that persists for several decades (Mantua and Hare, 2002). Over
115 the Indian Ocean, SST anomalies feature a seesaw structure between the western and
116 eastern equatorial regions, known as the Indian Ocean Dipole (IOD) mode (Saji et al.,
117 1999). The North Atlantic Ocean pronounces various modes of low-frequency SST
118 variability (Kushnir, 1994;Wu and Liu, 2005;Fan and Schneider, 2012;Taboada and
119 Anadon, 2012). The mechanisms responsible for SST variability includes ocean
120 circulation variability, wind stress, and ocean-atmosphere feedbacks (Frankignoul,
121 1985;Deser et al., 2010). Aerosols and greenhouse gases (GHGs) emitted from

anthropogenic and natural sources also contribute to regional SST variability through modulation of the solar radiation received by the ocean surface (Rotstayn and Lohmann, 2002;Wu and Kinter, 2011;Hsieh et al., 2013;Ding et al., 2014;Meehl et al., 2015).

Considering the distinct roles of regional SST variability in modulating regional climate systems, the impact of regional SST changes on the surface O_3 distribution needs to be explored. Lin et al. (2015) found that more frequent deep stratospheric intrusions appear over the western US during strong La Niña springs because of the meandering of the polar jet towards this region. This process can remarkably increase surface O_3 levels in the western US. The La Niña-like decadal cooling of the eastern equatorial Pacific Ocean in the 2000s weakened the long range transport of O_3-rich air from Eurasia towards Hawaii during spring (Lin et al., 2014). Liu et al. (2005) revealed that El Niño winters are associated with stronger transpacific pollutant transport, which also has implications for the long-range transport of O_3. Except for the ENSO impacts, very few studies to date have directly addressed the linkage between SST and O_3. Therefore, a comprehensive understanding of the response of surface O_3 to SST changes in individual ocean basins is lacking and necessary.

To fill this gap, this study focuses on examining the sensitivity of O_3 evolution over four polluted continental regions in the Northern Hemisphere (i.e., North America (NA, 15°N–55 °N; 60°W–125°W), Europe (EU, 25°N–65 °N; 10°W-50 °E), East Asia (EA, 15 °N–50 °N; 95°E–160 °E) and South Asia (SA, 5 °N–35 °N; 50 °E–95°E), defined in Fiore et al. (2009)) with respect to nearby basin-scale SST changes. We describe the design of numerical experiments and model configuration in Section 2. Surface O_3 responses to regional SST changes are given in Section 3. Relevant mechanisms governing the SST-O_3 relationships are discussed in Section 4. The impact of basin-scale SST changes on inter-continental transport of O_3 is described in Section 5. Conclusions are drawn in Section 6.

2. Methodology

2.1 Model description and configuration

The Community Earth System Model (CESM, v1.2.2) developed by the National Center for Atmospheric Research (NCAR) is used in this study, configured with the Community Atmosphere Model version 5.0 (CAM5) and the Community Land Model version 4.0 (CLM4). The ocean and sea ice components are prescribed with climatological SST and sea ice distributions. Moist turbulence is parameterized following the Bretherton and Park (2009) scheme. Shallow convection is parameterized using the Park and Bretherton (2009) scheme. The parameterization of deep convection is based on Zhang and McFarlane (1995) with modifications following Richter and Rasch (2008), Raymond and Blyth (1986), and Raymond and Blyth (1992). The cloud microphysical parameterization is following a two-moment scheme described in Morrison and Gettelman (2008) and Gettelman et al. (2008). The microphysical effect of aerosols on clouds are simulated following Ghan et al. (2012). The parameterization of cloud macrophysics follows Conley et al. (2012).

The chemistry coupled in the CAM5 (i.e., CAM5-chem) is primarily based on the Model for O_3 and Related chemical Tracers, version 4 (MOZART-4), which resolves 85 gas-phase species, and 196 gas-phase reactions (Emmons et al., 2010;Lamarque et al., 2012). A three-mode (i.e., Aitkin, accumulation and course) aerosol scheme for black carbon (BC), primary organic matter (POM), second organic aerosol (SOA), sea salt, dust and sulfate was used in our simulations following Liu and Ghan (2010). The lightning parameterization is modified according to Price et al. (1997) and tropospheric photolysis rates are calculated interactively following Tie et al. (2005). Gaseous dry deposition is calculated using the resistance-based parameterization of Wesely (1989), Walmsley and Wesely (1996), and Wesely and Hicks (2000). The parameterizations of in-cloud scavenging and below-cloud washout for soluble species are described in detail by Giorgi and Chameides (1985) and Brasseur et al. (1998), respectively. Anthropogenic emissions of chemical species are from the IPCC AR5 emission datasets (Lamarque et al., 2010), whose injection heights and particle size distributions follow the AEROCOM protocols (Dentener et al., 2006). The emissions of natural aerosols

and precursor gases are prescribed from the MOZART-2 (Horowitz et al., 2003) and MOZART-4 (Emmons et al., 2010) datasets. All emission datasets are available from the CESM data inventory (https://svn-ccsm-inputdata.cgd.ucar.edu/trunk/inputdata/). The performance of CESM in simulating tropospheric O_3 has been validated by comparing with ozonesondes and satellite observations (Tilmes et al., 2014). The deviations between model and observations are within the range of about 25%. In general, the model can capture the surface ozone distribution and variability well, but may overestimate O_3 over the Eastern US and Western Europe in the summer (Tilmes et al., 2014).

2.2 Numerical experiments

We first conduct a control simulation, hereafter referred to as CTRL, with prescribed climatological SSTs averaged from 1981 to 2010 (see Hurrell et al. (2008)). We then conduct six perturbation simulations with monthly SSTs that are uniformly increased or decreased by 1°C in three ocean basins in the Northern Hemisphere: the North Pacific (15°N-65°N; 100°E-90°W), North Atlantic (15°N-65°N; 100°W-20°E) and North Indian Oceans (5°N-30°N, 30°E-100°E; here 5°N is used to attain a relatively larger domain size). The simulations are denoted as “Pacific-W”, “Atlantic-W” and “Indian-W” for the three warming cases and “Pacific-C”, “Atlantic-C” and “Indian-C” for the three cooling cases. We defined the latitudinal and longitudinal ranges of these ocean basins mainly based on their geographical features. The boundaries of the prescribed SST anomalies generally align with the edge of the ocean basins, except along the southern side. In each perturbation simulation, we further linearly smooth the southern boundaries of these SST anomalies towards the equator to remove the sharp SST anomaly gradients at the edge，following a previous approach (e.g., Taschetto et al., 2016;Seager and Henderson, 2016). Air pollution emissions, including biogenic emissions of VOCs, are fixed to distinguish the impacts of SST variation on O_3 transport and photochemistry. All simulations are run for 21 years with the first year used for model spin-up.

To explore the impacts of SST changes on inter-continental transport, an explicit emission tagging technique is used in our simulations following previous studies (Shindell et al., 2008;Doherty et al., 2013). Artificial CO-like tracers emitted from four continental regions, i.e., North America (NA, 15°N–55 °N; 60°W–125°W), Europe (EU, 25°N–65 °N; 10°W-50 °E), East Asia (EA, 15 °N–50 °N; 95°E–160 °E) and South Asia (SA, 5 °N–35 °N; 50 °E–95°E), are tracked individually. These tracers are idealized with a first-order decay lifetime of 50 days, which is similar to O_3 (Doherty et al., 2013) and used to single out changes in O_3 transport induced by SST anomalies.

2.3 Integrated process rate (IPR) analysis

To provide a process-level explanation for the response of surface O_3 to regional SST changes, the IPR method is applied. This method calculates the accumulated contributions of individual processes (e.g., chemical production and loss, advection, vertical diffusion, dry deposition, etc.) to O_3 predictions during the model simulation and has been widely used for air pollution diagnostics (Li et al., 2012;Zhang and Wu, 2013;Tao et al., 2015). In this study, we added the IPR scheme to the CESM framework to track the contribution of six physicochemical processes (i.e., gas-phase chemistry (CHEM), advection (ADVE), vertical diffusion (VDIF), dry deposition (DRYD), shallow convection (SHAL) and deep convection (DEEP)) to O_3 concentrations in every grid box. Wet deposition and aqueous-phase chemistry are ignored here due to the low solubility and negligible chemical production of O_3 in water (Jacob, 1999). Therefore, CHEM represents the net production (production minus loss) rate of O_3 due to gas-phase photochemistry. DRYD represents the dry deposition fluxes of O_3, which is an important sink for O_3. The other IPR terms (i.e., ADVE, VDIF, SHAL and DEEP) represent contributions from different transport processes. The IPR scheme tracks and archives the O_3 flux in each grid from every process during each model time step. The sum of the O_3 fluxes from these six processes matches the change in the O_3 concentration. The IPR performance is verified by comparing the predicted hourly O_3 changes with the sum of the individual fluxes from the six processes. As shown in Figure S1, the hourly surface O_3 changes are well represented by the sum of these fluxes

in the model.

3. Response of surface O_3 concentrations to SST changes

Seasonally (i.e., DJF (December, January, February), MAM (March, April, May), JJA (June, July, August) and SON (September, October, November)) and regionally averaged surface O_3 changes in each SST perturbation simulation for the four highly populated continental regions and three ocean basins defined in our study are given in Tables 1 and S1, respectively. The responses of the surface O_3 concentrations to basin-scale SST changes (i.e., ±1 °C) are mainly below 3 ppbv in the Northern Hemisphere (Tables 1 and S1), though larger anomalies (i.e., up to 5 ppbv) are also observed over the eastern coast of China, the Indian subcontinent, and certain oceanic areas (Figures 1 and S3). This SST-O3 sensitivity is comparable to previous findings. For instance, Bloomer et al. (2009) reported a positive O_3-temperature relationship of 2.2~3.2 ppbv/°C across the rural eastern United States. Wu et al. (2008) found that summertime surface O_3 may increase by 2-5 ppbv over the northeastern United States in the 2050s. Additionally, Fiore et al. (2009) demonstrated an intercontinental decrease in surface O_3 of no more than 1 ppbv in response to 20 % reductions in anthropogenic emissions within a continental region. Our study indicates that basin-scale SST changes alone may exert significant effects on the surface O_3 above specific ocean basin and its surrounding continents.

As shown in Figure 1, seasonal changes of up to 5 ppbv in the mean surface O_3 concentration are observed during boreal summers, mainly in coastal regions and remote oceans. Surface O_3 changes in response to positive and negative SST anomalies generally pronounce a consistent spatial pattern but are opposite in sign, suggesting robust relationships between surface O_3 levels and SST anomalies (Figure 1). An increase in summertime SST over a specific ocean basin tends to increase the surface O_3 concentration over the upwind regions but reduce this concentration over downwind continents. For instance, a 1 °C warming over the North Pacific leads to a widespread

decrease in surface O_3 over the North Pacific, North America and the North Atlantic of approximately 1 ppbv (Table S1) but may enhance the surface O_3 by nearly 3 ppbv over South China. Similarly, in the "Atlantic-W" case, the surface O_3 levels decrease by 1~2 ppbv over the North Atlantic and Europe but increase (~1 ppbv) over North America and the North Pacific. For the North Indian Ocean, positive SST anomalies tend to increase the surface O_3 over the Indian Ocean and Africa but decrease the surface O_3 over South and East Asia (Figure 1). During the boreal winter, a widespread decrease in surface O_3 associated with the warming of different oceans is observed. Significant changes (e.g., up to 5 ppbv) mainly occur over remote ocean areas. Over populated continents, the response of the surface O_3 to basin-scale SST changes is typically insignificant. Details are shown in Figure S3 in the supplementary material.

Our simulations reveal that different oceans can exert distinct region-specific effects on the O_3 distribution. We further conduct two sensitivity tests with 1 °C SST warming and 1 °C SST cooling superimposed onto all three ocean basins (i.e., the North Pacific, North Atlantic and North Indian Ocean) in the Northern Hemisphere, denoted as "All-W" and "All-C", respectively. The effects of these combined warming and cooling cases on surface O_3 distributions are respectively compared with the sum of the three individual warming cases (i.e., Pacific-W, Atlantic-W and Indian-W) and three individual cooling cases (i.e., Pacific-C, Atlantic-C and Indian-C). The responses of surface O_3 to a hemispheric SST anomaly generally resemble the sum of responses to different regional SST changes (see Figures S5 and S7 in the supplementary material). We now analyze the processes that impact the dependence of SST on the O_3 distribution using simulations that increase the SST.

4. Mechanism of SST-induced surface O_3 changes

4.1 Process-level response to SST changes

IPR analysis is used to evaluate the contribution of different physicochemical processes to O_3 evolution. This type of analysis has been widely used in air quality studies to examine the cause of pollution episodes (Wang et al., 2010;Li et al., 2012). When

applied in climate sensitivity analysis (usually measuring the difference between two equilibriums), the net change of all IPRs approaches zero. Typically, the positive changes in IPRs are mainly responsible for the increase in surface O_3, which may further induce O_3 removal to balance this forcing in a new equilibrium. Therefore, here, the IPR analysis is used not to budget the SST-induced O_3 concentration changes but rather to help examine the relative importance of different transport and chemical processes in driving the sensitivity of O_3 to SST forcing. In this study, the SST-induced, process-level O_3 changes are spatially averaged over four populated continental regions (i.e., NA, EU, EA and SA, Figure 2) and three ocean basins (i.e., the North Pacific, North Atlantic and North Indian Oceans, Figure S9). In most cases, VDIF and DRYD are the key processes controlling the O_3 variation. The downward transport of O_3 through diffusion is an important source of surface O_3, while DRYD acts as a sink. Both processes are simultaneously determined by the strength of turbulence. Here, we define a new term TURB as the sum of DRYD and VDIF, which can capture the overall effect of turbulence changes on surface O_3 concentrations. In addition, we merge SHAL and DEEP as CONV to represent the total contribution of convective transport to surface O_3 (Figures 2 and S9). More detailed IPR results are shown in Figures S10 and S11 in the supplementary material.

In the "Pacific-W" case, a 1 °C SST warming over the North Pacific increases VDIF over eastern China in JJA (Figure S12), which is insignificant if averaged over the whole East Asia region. Meanwhile, this Pacific warming considerably reduces VDIF over North America (Figure S10). The corresponding decrease in TURB over North America mainly determines the surface O_3 reduction in JJA and SON, while the reduction in CONV exerts an additional negative impact (Figure 2). In the "Atlantic-W" case, increases in VDIF are also observed over the upwind regions (i.e., North America) in JJA. However, these increases are accompanied by commensurate decreases in DRYD, resulting in an insignificant overall change in TURB (Figure 2). Therefore, the increase in CHEM is mainly responsible for the surface O_3 increase over North America in JJA. TURB is more relatively important over Europe (only in JJA

and SON), leading to reduced surface O_3 abundance. In the "Indian-W" case, both CHEM and CONV are reduced over South Asia in JJA, leading to overall reductions in surface O_3 over the Indian subcontinent (Figure 2). The IPR analysis over the ocean basins shows that the warming of the North Pacific or North Atlantic induces reductions in VDIF and CHEM, which are responsible for the significant decrease in surface O_3 above these regions in JJA (Figure S11). The North Indian Ocean warming, on the other hand, enhances DEEP and VDIF, leading to a local increase in surface O_3 in JJA.

The IPR analysis indicates that, in general, an SST increase in the North Pacific or North Atlantic is more likely to enhance the vertical diffusion of O_3 over upwind regions (i.e., East Asia or North America, respectively) but suppress this diffusion over the ocean basin as well as downwind continents in JJA (Figure S12). These opposite changes in VDIF over upwind and downwind regions lead to distinct surface O_3 responses. Changes in CHEM enhance surface O_3 formation in most cases. An exception is in South Asia, where CHEM and DEEP dominate the reduction in surface O_3 over the region in JJA associated with the North Indian Ocean warming. In the following subsections, the mechanisms of the SST-O_3 relationship for the four polluted continents are further explored. Here we focus on boreal summers since the surface O_3 response to SST changes is more robust during this period than other seasons.

4.2 Response of photochemical O_3 production to SST increases

Changes in the net production rate (i.e., chemical production rate minus loss rate) of O_3 at the surface in JJA associated with basin-scale SST increases are shown in Figure 3. The peak changes are mainly confined to regions where O_3 precursors are abundant (e.g., South and East Asia and North America). For example, a warmer North Pacific SST exerts a positive (negative) impact on net O_3 production in the northern (southern) regions of East Asia. Similarly, the warming of the North Atlantic promotes a dipole impact on the surface O_3 production over North America, while the warming of the North Indian Ocean significantly decreases the net O_3 production rate over South Asia.

As emissions are fixed in all simulations, the change in net O_3 production is driven by SST induced meteorological changes (e.g., air temperature, air humidity, and solar radiation). An increase in SST of 1 °C in any ocean basin leads to a widespread enhancement of the surface air temperature (i.e., the air temperature at 2 m) over most continental areas (Figure 4). An exception is the North Indian Ocean, where an increase in SST tends to cool the Indian subcontinent by 1-2 °C. This temperature decrease is not only limited to the surface but also spreads to 600 hPa (Figure S16). Associated with this temperature decrease is a remarkable reduction in the solar radiation received at the continent below (more than 15 W/m^2, Figure S17). Previous studies have indicated that moist convection is more sensitive to the SST changes in the tropical oceans than in mid- or high- latitude oceans (Lau and Nath, 1994;Lau et al., 1997;Hartmann, 2015). The SST increase over the North Indian Ocean tends to strengthen the moist convection that eventually facilitates cloud formation in the upper troposphere (Roxy et al., 2015;Xi et al., 2015;Chaudhari et al., 2016). The latent heat released from convective activities significantly warms the air temperature over the upper troposphere (Sabeerali et al., 2012;Xi et al., 2015). Meanwhile, the corresponding increase in cloud cover blocks the solar radiation reaching the surface of the Indian subcontinent and reduce the air temperature of lower troposphere in that region. These processes lead to opposite air temperature changes between upper and lower troposphere over South Asia in response to the North Indian warming (as shown in Figure S16), which may further suppress the development of deep convection over the Indian subcontinent.

Previous studies have indicated that air temperature positively affects both O_3 production and destruction rates (Zeng et al., 2008;Pusede et al., 2015). As shown in Figure S19, changes in the net O_3 production rate are mainly dominated by O_3 production over continents but by O_3 destruction over oceans. An increase in SST leads to a widespread enhancement of the air temperature, resulting in a positive change in the net O_3 production over most continental regions (Figure 3). However, a warmer SST

388 also increases the air humidity (Figure S21), which enhances O_3 destruction over most
389 coastal and oceanic areas. In addition, over South Asia, a warming of the North Indian
390 Ocean decreases solar radiation and air temperature, and simultaneously increases air
391 humidity, which jointly exert negative effects on O_3 production in that region.
392

393 **4.3 Response of physical O_3 transport to SST increases**

394 In Section 4.1, our IPR analysis highlights multiple physical processes (i.e., vertical
395 diffusion, convection and advection) that are important in modulating surface O_3
396 concentrations. However, the role and relative importance of each process exhibit large
397 spatial heterogeneity. In this section, we explore the key factors controlling physical O_3
398 transport in response to basin-scale SST changes.
399

400 The changes in the surface pressure and wind pattern induced by a basin-wide SST
401 increase are shown in Figure 5. Generally, a warming of any ocean basin will lead to a
402 low-pressure anomaly centered to its west at low-latitudes, which is caused by SST-
403 induced convective activity. Additionally, the warming of the Indian Ocean induces an
404 anticyclonic anomaly over the subtropical western Pacific, which has been documented
405 in previous studies (Yang et al., 2007;Li et al., 2008). As shown in Figure 6, the surface
406 pressure reduction induced by SST warming in any ocean basin is closely associated
407 with enhanced upward motions, suggesting a substantial enhancement in deep
408 convection over tropical oceans. Previous studies have identified an SST threshold
409 (approximately 26°−28°C) to generating deep convection (Graham and Barnett,
410 1987;Johnson and Xie, 2010). Therefore, the sensitivity of deep convection to an SST
411 anomaly is strongly dependent on the distribution of base SST. The enhanced upward
412 motion in response to a uniform increase in basin-scale SST mainly occurs over regions
413 with high climatological SST (Figure 6). Regions with a low climatological SST have
414 little effects on the vertical movement of air masses.
415

416 Strengthened deep convection will trigger large-scale subsidence over nearby regions

through the modulation of large-scale circulation patterns, which may suppress convective transport (Lau et al., 1997;Roxy et al., 2015;Ueda et al., 2015). This effect is verified by the decreases in upward velocity at 500 hPa. As depicted in Figure 6, significant decreases in upward velocity occur over regions adjacent to the strengthened deep convection. Similar effects are also observed over higher latitudes or remote oceans (Figure S23). Meanwhile, the air temperature increase in response to regional SST warming is more significant above the lower troposphere, which leads to a decrease in the vertical temperature gradient (Figure S16). These factors tend to restrain the vertical exchange of air pollutants at mid-latitudes, which facilitates surface O_3 accumulation over polluted continental regions in JJA but may weaken the intrusion of O_3 from the upper troposphere to the surface in most unpolluted areas. This process helps to explain the widespread decrease in surface O_3 over unpolluted regions associated with an SST increase, as described in Section 3, and can be further verified by the wide-spread reduction in VDIF shown in Figure S12.

The surface pressure anomalies induced by SST changes can play a dominant role in modulating surface O_3 transport at specific locations. For example, the low-pressure anomaly centered over the subtropical northwestern Pacific in the "Pacific-W" case causes the convergence of wind in the lower troposphere (Figure 5a). Consequently, surface O_3 pollution is enhanced in southern China due to an increase in O_3 transport from more polluted northern China (Figure 7a). The vertical distribution of the corresponding O_3 changes also shows that the increase in O_3 over southern China occurs below 700hPa, accompanied by noticeable decreases above 700hPa as well as over nearby northern China (Figure 7d). The IPR analysis also indicates that the increases in advective transport and downward turbulent transport are mainly responsible for the surface O_3 increase in southern China.

In the "Atlantic-W" case, the SST warming-induced surface pressure anomalies lead to substantial O_3 redistribution, especially over the North Atlantic Ocean (Figure 7b). For North America, the changes in horizontal O_3 fluxes have no significant effect on the O_3

concentration increase. In addition, O_3 changes are observed to be larger in the upper troposphere than at the surface (Figure 7e). As demonstrated in Section 4.1, the response of lower-altitude O_3 over North America to the North Atlantic warming is mainly caused by enhanced chemical production, rather than physical transport.

The North Indian SST warming leads to a low-pressure anomaly centered over the Arabian Sea (Figure 5c). The warming of the North Indian Ocean strengthens the upward motion of air at low-latitudes and further induces a convergence of highly polluted air over the Indian Ocean. The effects of this process on O_3 concentrations are observed to be more significant in the upper troposphere (Figure 7f). According to the IPR analysis, the surface O_3 increase over the Indian Ocean is mainly caused by the enhanced vertical transport of O_3 to the surface through deep convection and vertical diffusion processes (Figure S11). However, over the nearby Indian subcontinent, the suppressed convection tends to decrease surface O_3 in that region (Figure 2).

5. Implications for O_3 long-range transport

The above findings indicate that, in general, a basin-scale SST increase in the Northern Hemisphere is more likely to enhance atmospheric stability at mid-latitudes, which may suppress air pollutants from lofting to the free troposphere. This process potentially has large effects on O_3 intercontinental transport. Following previous work (e.g., Doherty et al., 2013 ; Fang et al., 2011), we use passive CO-like tracers to demonstrate the potential effect of regional SST changes on long-range O_3 transport. A warming of North Pacific SSTs by 1°C tends to increase the East Asian CO tracer concentrations by nearly 6% at the surface (Figure 8b), which is accompanied by a significant reduction (~4%) in eastward transport to North America. Similarly, for the North American tracer, a warming of North Atlantic SSTs by 1°C increases (~1%) the concentrations in North America but decreases (3-4 %) the concentrations over downwind Europe (Figure 8d). The response of the South Asian CO tracer to North Indian Ocean warming also shows a decreasing tendency over downwind regions, but

the patterns are more complicated over the source region in this case (Figure 8e). Because the CO-like tracers added in the simulation have a fixed decay lifetime, their concentration changes are completely caused by the SST-induced transport anomalies. The decrease in CO tracer concentrations over downwind regions suggests that the warming of basin-scale SST tends to suppress the long-range transport of air pollutants. Additionally, in the "Pacific-W" case, changes in the East Asian CO tracer (Figure 8a) generally resemble the changes in surface O_3 over East Asia (Figure 7a), indicating the dominant effect of physical transport on the O_3 distribution over East Asia. Regarding the North American CO tracer in response to the North Atlantic warming or the South Asian CO tracer in response to the North Indian Ocean warming, their concentration changes are spatially inconsistent with those of O_3 (see Figures 7 and 8). This further indicates the distinct roles that different basin-scale SSTs play in nearby air quality.

Further investigations of zonal wind suggest that an increase in SST over different oceans consistently decreases the westerly winds at lower mid-latitudes (25°N - 45 °N) in the Northern Hemisphere but increases these winds at higher latitudes (Figure 9). In general, increases in the geopotential height induced by basin-scale SST warming are more significant at mid-latitudes than at other latitudes, which is consistent with the air temperature changes. Consequently, the meridional geopotential height gradient is decreasing at lower latitudes but increasing at higher latitudes, leading to corresponding changes in the westerly winds. The latitude band at 25°N - 45 °N covers many polluted regions (i.e., North America and East Asia). A weakened westerly wind may reduce long-rang O_3 transport. As demonstrated in Section 4.3, the basin-scale SST increases also exert negative effects on the upward transport of air masses at mid-latitudes. Therefore, the decreases in CO tracer concentrations over downwind regions (Figure 8a and 8c) can be explained by both suppressed vertical transport and weakened westerly winds. In the "Indian-W" case, the SST increase over North India leads to a low-pressure anomaly above the Arabian Sea due to the enhanced deep convection (as discussed in Section 4.3). The corresponding anomalous cyclone should be responsible for the dipole of the South Asian CO tracer changes over the source region depicted in

Figure 8e.

In addition, we also find a hemispheric-scale decrease in peroxyacetyl nitrate (PAN), a reservoir of O_3 precursors (NO_X and HO_X) that facilitates the long-range transport of O_3, during the warming of different oceans (Figure S25). This decrease is likely caused by the increase in the thermal decomposition of PAN in response to the air temperature increase (Jacob and Winner, 2009;Doherty et al., 2013).

Thus, it is reasonable to infer that, in general, the increased thermal decomposition of PAN, the weakened mid-latitude westerlies, and the reduced vertical air transport may exert a joint reducing effect on the intercontinental transport of O_3 during basin-scale SST increases.

6. Summary

In this paper, we investigate the responses of surface O_3 to basin-scale SST anomalies in the Northern Hemisphere. The latest version of CESM (version 1.2.2) is used in our simulation, forced with climatological and stationary SST anomalies (± 1 °C) in the North Pacific, North Atlantic and North Indian Oceans, respectively. The responses of surface O_3 associated with these SST changes are evaluated. Results of similar magnitude but opposite sign are observed for the SST warming versus cooling simulations for each ocean basin, suggesting robust connections between the SST anomalies and surface O_3 changes. The regionally and seasonally averaged surface O_3 changes over four continental regions (i.e., NA, EU, EA and SA) pronounce wide seasonal and regional variability (varying from 1 to 3 ppbv). The warming of the North Pacific leads to nearly 3 ppbv increases in the surface O_3 over southern China in summer, with corresponding decreases over North America (~1 ppbv). Similarly, the North Atlantic SST warming elevates the surface O_3 pollution over North America while reducing the surface O_3 (nearly 1-2 ppbv) over Europe. Changes in the North Indian SST exert significant impacts (1-3 ppbv) over South and East Asia during the entire

year.

Process analysis indicates that dry deposition and vertical diffusion are two major processes governing the surface O_3 balance. The increase in SST in different ocean basins tends to increase the contributions of vertical diffusion to surface O_3 over upwind regions while greatly restraining that over downwind continents. These processes generally lead to widespread decreases in surface O_3, which are partially offset by increases in air temperature-dependent chemical production rates. Specifically, the chemical production changes are mainly responsible for the surface O_3 increases over North America in response to the North Atlantic SST warming but exert a negative effect on South Asia in response to the North Indian SST warming. Decreases in the convective transport of O_3 to the surface associated with North Indian warming are significant over South Asia and exert a negative impact on surface O_3 concentrations. Advective transport has a positive effect on surface O_3 in southern China in the "Pacific-W" case.

We further show that air temperature is an important factor controlling the surface O_3 responses to SST anomalies. Reductions in the surface O_3 chemical production in South Asia associated with North Indian SST warming can be explained by the corresponding SST-induced decreases in ground-level air temperature and solar radiation. Meanwhile, the widespread increase in air temperature associated with basin-scale SST warming is more likely to promote O_3 production over other highly polluted regions.

On the other hand, SST increases at low latitudes over different oceans enhance deep convection in summer, which promotes convergence at the surface, as well as upward motions at low latitudes. The corresponding surface pressure anomalies centered over the east coast of East Asia associated with the North Pacific warming and over the Arabian Sea associated with the North Indian warming tend to increase the surface O_3 above through exchanges with the surrounding highly polluted air. The basin-scale SST increases in the Northern Hemisphere reduce the tropospheric temperature gradient at

mid-latitudes that restrains vertical transport of O_3 over continents and weakens the westerlies at lower mid-latitudes. The response of the CO-tracer also suggests that these factors may jointly exert a negative effect on the intercontinental transport of O_3.

Overall, our study highlights the sensitivity of O_3 evolution to basin-wide SST changes in the Northern Hemisphere and identifies the key chemical or dynamical factors that control this evolution. However, to provide a more comprehensive understanding of the SST-O_3 relationship, further studies using realistic SST variability are necessary. This study may aid in the management of O_3 pollution by considering the influence of specific SST variability.

Acknowledgements

This work was supported by funding from the National Natural Science Foundation of China under awards 41671491, 41571130010, and 41390240, National Key Research and Development Program of China 2016YFC0206202, and the 111 Project (B14001). This work was also supported in part by the National Science Foundation under grant CBET-1512429.

References:

Auvray, M., and Bey, I.: Long‐range transport to Europe: Seasonal variations and implications for the European ozone budget, Journal of Geophysical Research: Atmospheres (1984–2012), 110, 2005.

Barnes, E. A., and Fiore, A. M.: Surface ozone variability and the jet position: Implications for projecting future air quality, Geophys Res Lett, 40, 2839-2844, 2013.

Bloomer, B. J., Stehr, J. W., Piety, C. A., Salawitch, R. J., and Dickerson, R. R.: Observed relationships of ozone air pollution with temperature and emissions, Geophys Res Lett, 36, 2009.

Brasseur, G., Hauglustaine, D., Walters, S., Rasch, P., Müller, J. F., Granier, C., and Tie, X.: MOZART, a global chemical transport model for ozone and related chemical tracers: 1. Model description, Journal of Geophysical Research: Atmospheres, 103, 28265-28289, 1998.

Bretherton, C. S., and Park, S.: A new moist turbulence parameterization in the Community Atmosphere Model, J Climate, 22, 3422-3448, 2009.

Bronnimann, S., Luterbacher, J., Schmutz, C., Wanner, H., and Staehelin, J.: Variability of total ozone at Arosa, Switzerland, since 1931 related to atmospheric circulation indices, Geophys Res Lett, 27, 2213-2216, 2000.

599 Brown-Steiner, B., and Hess, P.: Asian influence on surface ozone in the United States: A comparison of
600 chemistry, seasonality, and transport mechanisms, J Geophys Res-Atmos, 116, Artn D17309
601 10.1029/2011jd015846, 2011.
602 Brown, J., and Bowman, C.: Integrated Science Assessment for Ozone and Related Photochemical
603 Oxidants, EPA 600/R-10, 2013.
604 Camalier, L., Cox, W., and Dolwick, P.: The effects of meteorology on ozone in urban areas and their use
605 in assessing ozone trends, Atmos Environ, 41, 7127-7137, 2007.
606 Chaudhari, H. S., Pokhrel, S., Kulkarni, A., Hazra, A., and Saha, S. K.: Clouds–SST relationship and
607 interannual variability modes of Indian summer monsoon in the context of clouds and SSTs:
608 observational and modelling aspects, Int J Climatol, 36, 4723-4740, 2016.
609 Christoudias, T., Pozzer, A., and Lelieveld, J.: Influence of the North Atlantic Oscillation on air pollution
610 transport, Atmos Chem Phys, 12, 869-877, 2012.
611 Chuwah, C., van Noije, T., van Vuuren, D. P., Stehfest, E., and Hazeleger, W.: Global impacts of surface
612 ozone changes on crop yields and land use, Atmos Environ, 106, 11-23,
613 10.1016/j.atmosenv.2015.01.062, 2015.
614 Conley, A. J., Garcia, R., Kinnison, D., Lamarque, J.-F., Marsh, D., Mills, M., Smith, A. K., Tilmes, S., Vitt, F.,
615 and Morrison, H.: Description of the NCAR community atmosphere model (CAM 5.0), NCAR
616 technical note, 2012.
617 Creilson, J., Fishman, J., and Wozniak, A.: Intercontinental transport of tropospheric ozone: a study of
618 its seasonal variability across the North Atlantic utilizing tropospheric ozone residuals and its
619 relationship to the North Atlantic Oscillation, Atmos Chem Phys, 3, 2053-2066, 2003.
620 Dentener, F., Kinne, S., Bond, T., Boucher, O., Cofala, J., Generoso, S., Ginoux, P., Gong, S., Hoelzemann,
621 J., and Ito, A.: Emissions of primary aerosol and precursor gases in the years 2000 and 1750
622 prescribed data-sets for AeroCom, Atmos Chem Phys, 6, 4321-4344, 2006.
623 Deser, C., Alexander, M. A., Xie, S.-P., and Phillips, A. S.: Sea surface temperature variability: Patterns
624 and mechanisms, Annual Review of Marine Science, 2, 115-143, 2010.
625 Ding, Y., Carton, J. A., Chepurin, G. A., Stenchikov, G., Robock, A., Sentman, L. T., and Krasting, J. P.: Ocean
626 response to volcanic eruptions in Coupled Model Intercomparison Project 5 simulations, Journal
627 of Geophysical Research: Oceans, 119, 5622-5637, 2014.
628 Doherty, R. M., Wild, O., Shindell, D. T., Zeng, G., MacKenzie, I. A., Collins, W. J., Fiore, A. M., Stevenson,
629 D. S., Dentener, F. J., Schultz, M. G., Hess, P., Derwent, R. G., and Keating, T. J.: Impacts of climate
630 change on surface ozone and intercontinental ozone pollution: A multi-model study, J Geophys
631 Res-Atmos, 118, 3744-3763, 10.1002/jgrd.50266, 2013.
632 Emmons, L., Walters, S., Hess, P., Lamarque, J.-F., Pfister, G., Fillmore, D., Granier, C., Guenther, A.,
633 Kinnison, D., and Laepple, T.: Description and evaluation of the Model for Ozone and Related
634 chemical Tracers, version 4 (MOZART-4), Geoscientific Model Development, 3, 43-67, 2010.
635 Fan, M., and Schneider, E. K.: Observed decadal North Atlantic tripole SST variability. Part I: weather
636 noise forcing and coupled response, J Atmos Sci, 69, 35-50, 2012.
637 Fang, Y., Fiore, A. M., Horowitz, L. W., Gnanadesikan, A., Held, I., Chen, G., Vecchi, G., and Levy, H.: The
638 impacts of changing transport and precipitation on pollutant distributions in a future climate,
639 Journal of Geophysical Research: Atmospheres, 116, 2011.
640 Fehsenfeld, F., Daum, P., Leaitch, W., Trainer, M., Parrish, D., and Hübler, G.: Transport and processing of
641 O3 and O3 precursors over the North Atlantic: An overview of the 1993 North Atlantic Regional
642 Experiment (NARE) summer intensive, Journal of Geophysical Research: Atmospheres, 101,

643 28877-28891, 1996.
644 Fiore, A., Dentener, F., Wild, O., Cuvelier, C., Schultz, M., Hess, P., Textor, C., Schulz, M., Doherty, R., and
645 Horowitz, L.: Multimodel estimates of intercontinental source‐receptor relationships for ozone
646 pollution, Journal of Geophysical Research: Atmospheres (1984–2012), 114, 2009.
647 Frankignoul, C.: Sea surface temperature anomalies, planetary waves, and air‐sea feedback in the
648 middle latitudes, Reviews of geophysics, 23, 357-390, 1985.
649 Frankignoul, C., and Sennéchael, N.: Observed influence of North Pacific SST anomalies on the
650 atmospheric circulation, J Climate, 20, 592-606, 2007.
651 Gettelman, A., Morrison, H., and Ghan, S. J.: A new two-moment bulk stratiform cloud microphysics
652 scheme in the Community Atmosphere Model, version 3 (CAM3). Part II: Single-column and
653 global results, J Climate, 21, 3660-3679, 2008.
654 Ghan, S. J., Liu, X., Easter, R. C., Zaveri, R., Rasch, P. J., Yoon, J.-H., and Eaton, B.: Toward a minimal
655 representation of aerosols in climate models: Comparative decomposition of aerosol direct,
656 semidirect, and indirect radiative forcing, J Climate, 25, 6461-6476, 2012.
657 Giorgi, F., and Chameides, W.: The rainout parameterization in a photochemical model, Journal of
658 Geophysical Research: Atmospheres, 90, 7872-7880, 1985.
659 Glantz, M. H., Katz, R. W., and Nicholls, N.: Teleconnections linking worldwide climate anomalies,
660 Cambridge University Press Cambridge, 1991.
661 Goswami, B., Madhusoodanan, M., Neema, C., and Sengupta, D.: A physical mechanism for North
662 Atlantic SST influence on the Indian summer monsoon, Geophys Res Lett, 33, 2006.
663 Graham, N., and Barnett, T.: Sea surface temperature, surface wind divergence, and convection over
664 tropical oceans, Science, 238, 657-659, 1987.
665 Grewe, V.: The origin of ozone, Atmos Chem Phys, 6, 1495-1511, 2006.
666 Guenther, R.: Isoprene and monoterpene emission rate variability: model evaluations and sensitivity
667 analyses, J Geophys Res, 98, 1993.
668 Gulev, S. K., Latif, M., Keenlyside, N., Park, W., and Koltermann, K. P.: North Atlantic Ocean control on
669 surface heat flux on multidecadal timescales, Nature, 499, 464-467, 2013.
670 Hartmann, D. L.: Pacific sea surface temperature and the winter of 2014, Geophys Res Lett, 42, 1894-
671 1902, 2015.
672 Hess, P., and Mahowald, N.: Interannual variability in hindcasts of atmospheric chemistry: the role of
673 meteorology, Atmos. Chem. Phys, 9, 5261-5280, 2009.
674 Horowitz, L. W., Walters, S., Mauzerall, D. L., Emmons, L. K., Rasch, P. J., Granier, C., Tie, X., Lamarque, J.
675 F., Schultz, M. G., and Tyndall, G. S.: A global simulation of tropospheric ozone and related tracers:
676 Description and evaluation of MOZART, version 2, Journal of Geophysical Research: Atmospheres
677 (1984–2012), 108, 2003.
678 Hsieh, W. C., Collins, W. D., Liu, Y., Chiang, J. C. H., Shie, C. L., Caldeira, K., and Cao, L.: Climate response
679 due to carbonaceous aerosols and aerosol-induced SST effects in NCAR community atmospheric
680 model CAM3.5, Atmos Chem Phys, 13, 7489-7510, DOI 10.5194/acp-13-7489-2013, 2013.
681 Hurrell, J. W., Hack, J. J., Shea, D., Caron, J. M., and Rosinski, J.: A new sea surface temperature and sea
682 ice boundary dataset for the Community Atmosphere Model, J Climate, 21, 5145-5153, 2008.
683 Jacob, D.: Introduction to atmospheric chemistry, Princeton University Press, 1999.
684 Jacob, D. J., and Winner, D. A.: Effect of climate change on air quality, Atmos Environ, 43, 51-63, 2009.
685 Jiang, Z., Miyazaki, K., Worden, J. R., Liu, J. J., Jones, D., and Henze, D. K.: Impacts of anthropogenic and
686 natural sources on free tropospheric ozone over the Middle East, Atmos Chem Phys, 16, 6537-

687 6546, 2016.
688 Johnson, C., Collins, W., Stevenson, D., and Derwent, R.: Relative roles of climate and emissions changes
689 on future tropospheric oxidant concentrations, Journal of Geophysical Research: Atmospheres
690 (1984–2012), 104, 18631-18645, 1999.
691 Johnson, N. C., and Xie, S.-P.: Changes in the sea surface temperature threshold for tropical convection,
692 Nat Geosci, 3, 842-845, 2010.
693 Knowland, K., Doherty, R., and Hodges, K. I.: The effects of springtime mid-latitude storms on trace gas
694 composition determined from the MACC reanalysis, Atmos Chem Phys, 15, 3605-3628, 2015.
695 Kushnir, Y.: Interdecadal variations in North Atlantic sea surface temperature and associated
696 atmospheric conditions, J Climate, 7, 141-157, 1994.
697 Kushnir, Y., Robinson, W., Bladé, I., Hall, N., Peng, S., and Sutton, R.: Atmospheric GCM response to
698 extratropical SST anomalies: Synthesis and evaluation*, J Climate, 15, 2233-2256, 2002.
699 Lamarque, J.-F., Bond, T. C., Eyring, V., Granier, C., Heil, A., Klimont, Z., Lee, D., Liousse, C., Mieville, A.,
700 and Owen, B.: Historical (1850–2000) gridded anthropogenic and biomass burning emissions of
701 reactive gases and aerosols: methodology and application, Atmos Chem Phys, 10, 7017-7039,
702 2010.
703 Lamarque, J., Emmons, L., Hess, P., Kinnison, D. E., Tilmes, S., Vitt, F., Heald, C., Holland, E. A., Lauritzen,
704 P., and Neu, J.: CAM-chem: Description and evaluation of interactive atmospheric chemistry in
705 the Community Earth System Model, Geosci. Model Dev, 5, 369-411, 2012.
706 Lamarque, J. F., and Hess, P. G.: Arctic Oscillation modulation of the Northern Hemisphere spring
707 tropospheric ozone, Geophys Res Lett, 31, 2004.
708 Lau, K., Wu, H., and Bony, S.: The role of large-scale atmospheric circulation in the relationship between
709 tropical convection and sea surface temperature, J Climate, 10, 381-392, 1997.
710 Lau, N.-C., and Nath, M. J.: A modeling study of the relative roles of tropical and extratropical SST
711 anomalies in the variability of the global atmosphere-ocean system, J Climate, 7, 1184-1207,
712 1994.
713 Lau, N.-C.: Interactions between global SST anomalies and the midlatitude atmospheric circulation, B
714 Am Meteorol Soc, 78, 21-33, 1997.
715 Li, L., Chen, C., Huang, C., Huang, H., Zhang, G., Wang, Y., Wang, H., Lou, S., Qiao, L., and Zhou, M.:
716 Process analysis of regional ozone formation over the Yangtze River Delta, China using the
717 Community Multi-scale Air Quality modeling system, Atmos Chem Phys, 12, 10971-10987, 2012.
718 Li, S., Lu, J., Huang, G., and Hu, K.: Tropical Indian Ocean basin warming and East Asian summer monsoon:
719 A multiple AGCM study, J Climate, 21, 6080-6088, 2008.
720 Lin, M., Fiore, A. M., Horowitz, L. W., Cooper, O. R., Naik, V., Holloway, J., Johnson, B. J., Middlebrook, A.
721 M., Oltmans, S. J., and Pollack, I. B.: Transport of Asian ozone pollution into surface air over the
722 western United States in spring, Journal of Geophysical Research: Atmospheres, 117, 2012a.
723 Lin, M., Horowitz, L. W., Oltmans, S. J., Fiore, A. M., and Fan, S.: Tropospheric ozone trends at Mauna
724 Loa Observatory tied to decadal climate variability, Nat Geosci, 7, 136-143, 2014.
725 Lin, M., Fiore, A. M., Horowitz, L. W., Langford, A. O., Oltmans, S. J., Tarasick, D., and Rieder, H. E.: Climate
726 variability modulates western US ozone air quality in spring via deep stratospheric intrusions,
727 Nat Commun, 6, 2015.
728 Lin, M. Y., Fiore, A. M., Cooper, O. R., Horowitz, L. W., Langford, A. O., Levy, H., Johnson, B. J., Naik, V.,
729 Oltmans, S. J., and Senff, C. J.: Springtime high surface ozone events over the western United
730 States: Quantifying the role of stratospheric intrusions, J Geophys Res-Atmos, 117, Artn D00v22

731 10.1029/2012jd018151, 2012b.
732 Liu, J., Mauzerall, D. L., and Horowitz, L. W.: Analysis of seasonal and interannual variability in
733 transpacific transport, Journal of Geophysical Research: Atmospheres, 110, 2005.
734 Liu, X., and Ghan, S.: A modal aerosol model implementation in the community atmosphere model,
735 version 5 (CAM5), J. Atmos. Sci, 2010.
736 Mantua, N. J., and Hare, S. R.: The Pacific decadal oscillation, J Oceanogr, 58, 35-44, 2002.
737 Meehl, G. A., Teng, H., Maher, N., and England, M. H.: Effects of the Mount Pinatubo eruption on decadal
738 climate prediction skill of Pacific sea surface temperatures, Geophys Res Lett, 42, 2015.
739 Morrison, H., and Gettelman, A.: A new two-moment bulk stratiform cloud microphysics scheme in the
740 Community Atmosphere Model, version 3 (CAM3). Part I: Description and numerical tests, J
741 Climate, 21, 3642-3659, 2008.
742 Ordónez, C., Mathis, H., Furger, M., Henne, S., Hüglin, C., Staehelin, J., and Prévôt, A.: Changes of daily
743 surface ozone maxima in Switzerland in all seasons from 1992 to 2002 and discussion of summer
744 2003, Atmos Chem Phys, 5, 1187-1203, 2005.
745 Organization, W. H.: Review of evidence on health aspects of air pollution–REVIHAAP Project, World
746 Health Organization, Copenhagen, Denmark, 2013.
747 Park, S., and Bretherton, C. S.: The University of Washington shallow convection and moist turbulence
748 schemes and their impact on climate simulations with the Community Atmosphere Model, J
749 Climate, 22, 3449-3469, 2009.
750 Parrish, D. D., Holloway, J. S., Trainer, M., Murphy, P. C., Fehsenfeld, F. C., and Forbes, G. L.: Export of
751 North American ozone pollution to the north Atlantic Ocean, Science, 259, 1436-1439, 1993.
752 Pausata, F. S., Pozzoli, L., Vignati, E., and Dentener, F. J.: North Atlantic Oscillation and tropospheric
753 ozone variability in Europe: model analysis and measurements intercomparison, Atmos Chem
754 Phys, 12, 6357-6376, 2012.
755 Peñuelas, J., and Llusià, J.: The complexity of factors driving volatile organic compound emissions by
756 plants, Biologia Plantarum, 44, 481-487, 2001.
757 Philander, S. G. H.: El Niño southern oscillation phenomena, Nature, 302, 295-301, 1983.
758 Price, C., Penner, J., and Prather, M.: NOx from lightning: 1. Global distribution based on lightning physics,
759 Journal of Geophysical Research: Atmospheres (1984–2012), 102, 5929-5941, 1997.
760 Pusede, S. E., Steiner, A. L., and Cohen, R. C.: Temperature and recent trends in the chemistry of
761 continental surface ozone, Chem Rev, 115, 3898-3918, 2015.
762 Rasmussen, D. J., Fiore, A. M., Naik, V., Horowitz, L. W., McGinnis, S. J., and Schultz, M. G.: Surface ozone-
763 temperature relationships in the eastern US: A monthly climatology for evaluating chemistry-
764 climate models, Atmos Environ, 47, 142-153, 10.1016/j.atmosenv.2011.11.021, 2012.
765 Raymond, D., and Blyth, A.: Extension of the stochastic mixing model to cumulonimbus clouds, J Atmos
766 Sci, 49, 1968-1983, 1992.
767 Raymond, D. J., and Blyth, A. M.: A stochastic mixing model for nonprecipitating cumulus clouds, J Atmos
768 Sci, 43, 2708-2718, 1986.
769 Richter, J. H., and Rasch, P. J.: Effects of convective momentum transport on the atmospheric circulation
770 in the Community Atmosphere Model, version 3, J Climate, 21, 1487-1499, 2008.
771 Rotstayn, L. D., and Lohmann, U.: Tropical rainfall trends and the indirect aerosol effect, J Climate, 15,
772 2103-2116, 2002.
773 Roxy, M. K., Ritika, K., Terray, P., Murtugudde, R., Ashok, K., and Goswami, B.: Drying of Indian
774 subcontinent by rapid Indian Ocean warming and a weakening land-sea thermal gradient, Nat

775 Commun, 6, 2015.
776 Sabeerali, C., Rao, S. A., Ajayamohan, R., and Murtugudde, R.: On the relationship between Indian
777 summer monsoon withdrawal and Indo-Pacific SST anomalies before and after 1976/1977
778 climate shift, Clim Dynam, 39, 841-859, 2012.
779 Saji, N., Goswami, B., Vinayachandran, P., and Yamagata, T.: A dipole mode in the tropical Indian Ocean,
780 Nature, 401, 360-363, 1999.
781 Seager, R., and Henderson, N.: On the Role of Tropical Ocean Forcing of the Persistent North American
782 West Coast Ridge of Winter 2013/14 a, J Climate, 29, 8027-8049, 2016.
783 Shindell, D., Chin, M., Dentener, F., Doherty, R., Faluvegi, G., Fiore, A. M., Hess, P., Koch, D., MacKenzie,
784 I., and Sanderson, M.: A multi-model assessment of pollution transport to the Arctic, Atmos
785 Chem Phys, 8, 5353-5372, 2008.
786 Sillman, S., and Samson, P. J.: Impact of temperature on oxidant photochemistry in urban, polluted rural
787 and remote environments, Journal of Geophysical Research: Atmospheres, 100, 11497-11508,
788 1995.
789 Simmonds, P., Derwent, R., Manning, A., and Spain, G.: Significant growth in surface ozone at Mace
790 Head, Ireland, 1987–2003, Atmos Environ, 38, 4769-4778, 2004.
791 Simon, H., Reff, A., Wells, B., Xing, J., and Frank, N.: Ozone trends across the United States over a period
792 of decreasing NOx and VOC emissions, Environ Sci Technol, 49, 186-195, 2014.
793 Small, R., Xie, S., O'Neill, L., Seo, H., Song, Q., Cornillon, P., Spall, M., and Minobe, S.: Air–sea interaction
794 over ocean fronts and eddies, Dynam Atmos Oceans, 45, 274-319, 2008.
795 Sutton, R. T., and Hodson, D. L.: Atlantic Ocean forcing of North American and European summer climate,
796 Science, 309, 115-118, 2005.
797 Sutton, R. T., and Hodson, D. L.: Climate response to basin-scale warming and cooling of the North
798 Atlantic Ocean, J Climate, 20, 891-907, 2007.
799 Taboada, F. G., and Anadon, R.: Patterns of change in sea surface temperature in the North Atlantic
800 during the last three decades: beyond mean trends, Climatic Change, 115, 419-431, 2012.
801 Tao, W., Liu, J., Ban-Weiss, G., Hauglustaine, D., Zhang, L., Zhang, Q., Cheng, Y., Yu, Y., and Tao, S.: Effects
802 of urban land expansion on the regional meteorology and air quality of eastern China, Atmos
803 Chem Phys, 15, 8597-8614, 2015.
804 Taschetto, A., Rodrigues, R., Meehl, G., McGregor, S., and England, M.: How sensitive are the Pacific–
805 tropical North Atlantic teleconnections to the position and intensity of El Niño-related warming?,
806 Clim Dynam, 46, 1841-1860, 2016.
807 Tie, X., Madronich, S., Walters, S., Edwards, D. P., Ginoux, P., Mahowald, N., Zhang, R., Lou, C., and
808 Brasseur, G.: Assessment of the global impact of aerosols on tropospheric oxidants, Journal of
809 Geophysical Research: Atmospheres, 110, 2005.
810 Tilmes, S., Lamarque, J.-F., Emmons, L., Kinnison, D., Ma, P.-L., Liu, X., Ghan, S., Bardeen, C., Arnold, S.,
811 and Deeter, M.: Description and evaluation of tropospheric chemistry and aerosols in the
812 Community Earth System Model (CESM1. 2), Geoscientific Model Development Discussions, 7,
813 8875-8940, 2014.
814 Ueda, H., Kamae, Y., Hayasaki, M., Kitoh, A., Watanabe, S., Miki, Y., and Kumai, A.: Combined effects of
815 recent Pacific cooling and Indian Ocean warming on the Asian monsoon, Nat Commun, 6, 2015.
816 Vingarzan, R.: A review of surface ozone background levels and trends, Atmos Environ, 38, 3431-3442,
817 2004.
818 Walmsley, J. L., and Wesely, M. L.: Modification of coded parametrizations of surface resistances to

gaseous dry deposition, Atmos Environ, 30, 1181-1188, 1996.
Wang, B., Wu, R., and Fu, X.: Pacific-East Asian teleconnection: how does ENSO affect East Asian climate?, J Climate, 13, 1517-1536, 2000.
Wang, C., Deser, C., Yu, J.-Y., DiNezio, P., and Clement, A.: El Nino and southern oscillation (ENSO): a review, Coral Reefs of the Eastern Pacific, 3-19, 2012.
Wang, X., Zhang, Y., Hu, Y., Zhou, W., Lu, K., Zhong, L., Zeng, L., Shao, M., Hu, M., and Russell, A.: Process analysis and sensitivity study of regional ozone formation over the Pearl River Delta, China, during the PRIDE-PRD2004 campaign using the Community Multiscale Air Quality modeling system, Atmos Chem Phys, 10, 4423-4437, 2010.
Webster, P. J.: Mechanisms determining the atmospheric response to sea surface temperature anomalies, J Atmos Sci, 38, 554-571, 1981.
Wesely, M.: Parameterization of surface resistances to gaseous dry deposition in regional-scale numerical models, Atmospheric Environment (1967), 23, 1293-1304, 1989.
Wesely, M., and Hicks, B.: A review of the current status of knowledge on dry deposition, Atmos Environ, 34, 2261-2282, 2000.
Wild, O., and Akimoto, H.: Intercontinental transport of ozone and its precursors in a three-dimensional global CTM, Journal of Geophysical Research: Atmospheres, 106, 27729-27744, 2001.
Wu, L., and Liu, Z.: North Atlantic Decadal Variability: Air-Sea Coupling, Oceanic Memory, and Potential Northern Hemisphere Resonance*, J Climate, 18, 331-349, 2005.
Wu, R. G., and Kinter, J. L.: Shortwave radiation-SST relationship over the mid-latitude North Pacific during boreal summer in climate models, Clim Dynam, 36, 2251-2264, DOI 10.1007/s00382-010-0775-5, 2011.
Wu, S., Mickley, L. J., Leibensperger, E. M., Jacob, D. J., Rind, D., and Streets, D. G.: Effects of 2000–2050 global change on ozone air quality in the United States, Journal of Geophysical Research: Atmospheres, 113, 2008.
Xi, J., Zhou, L., Murtugudde, R., and Jiang, L.: Impacts of intraseasonal sst anomalies on precipitation during Indian summer monsoon, J Climate, 28, 4561-4575, 2015.
Yang, J., Liu, Q., Xie, S. P., Liu, Z., and Wu, L.: Impact of the Indian Ocean SST basin mode on the Asian summer monsoon, Geophys Res Lett, 34, 2007.
Zeng, G., Pyle, J., and Young, P.: Impact of climate change on tropospheric ozone and its global budgets, Atmos Chem Phys, 8, 369-387, 2008.
Zhang, G. J., and McFarlane, N. A.: Sensitivity of climate simulations to the parameterization of cumulus convection in the Canadian Climate Centre general circulation model, Atmos Ocean, 33, 407-446, 1995.
Zhang, L., Jacob, D. J., Yue, X., Downey, N. V., Wood, D. A., and Blewitt, D.: Sources contributing to background surface ozone in the US Intermountain West, Atmos Chem Phys, 14, 5295-5309, 10.5194/acp-14-5295-2014, 2014.
Zhang, Y., and Wu, S.-Y.: Understanding of the Fate of Atmospheric Pollutants Using a Process Analysis Tool in a 3-D Regional Air Quality Model at a Fine Grid Scale, Atmospheric and Climate Sciences, 3, 18, 2013.

Table 1. Regionally and seasonally averaged (only land grid boxes are included) changes in surface O_3 concentrations (ppbv) for basin-scale SST perturbation cases relative to the control simulation. Positive (negative) changes that are significant at the 0.05 level evaluated by Student's t-test are marked in red (blue).

Ozone (ppbv)			DJF	MAM	JJA	SON
North Pacific	+1° C	North America	-0.27*	-0.42*	-0.92*	-1.03*
		Europe	-0.50*	-0.26	0.10	-0.29
		East Asia	-0.88*	-0.71*	0.20	0.17
		South Asia	-1.00*	0.30	0.43	0.43*
	-1° C	North America	0.00	0.57*	0.55*	0.82*
		Europe	0.19	0.15	-0.47*	0.47*
		East Asia	0.30	-0.17	-0.22	-0.67*
		South Asia	0.04	-0.24	0.03	-0.40
North Atlantic	+1° C	North America	0.03	0.49	0.50*	0.53*
		Europe	0.30*	0.06	-1.61*	-0.89*
		East Asia	-0.52*	-0.68*	-0.62*	-0.25
		South Asia	-0.20	-1.46*	-1.28*	-0.82*
	-1° C	North America	-0.07	-0.10	0.10	-0.17
		Europe	0.00	0.00	0.07	0.06
		East Asia	0.16	-0.08	0.80*	-0.60*
		South Asia	-0.20	-0.40	0.30	-0.10
North India	+1° C	North America	-0.25	-0.04	-0.16	-0.10
		Europe	-0.30	0.08	-0.12	0.19
		East Asia	-0.53*	-0.77*	-0.28	-1.78*
		South Asia	-1.00*	0.14	-1.67*	-2.75*
	-1° C	North America	0.04	0.17	0.04	0.25
		Europe	0.05	-0.07	-0.13	-0.24
		East Asia	-0.06	0.15	0.55*	0.33
		South Asia	-0.03	0.57	1.70*	1.31*

*Significant at the 0.05 level from Student's t-test using 20 years of model results.

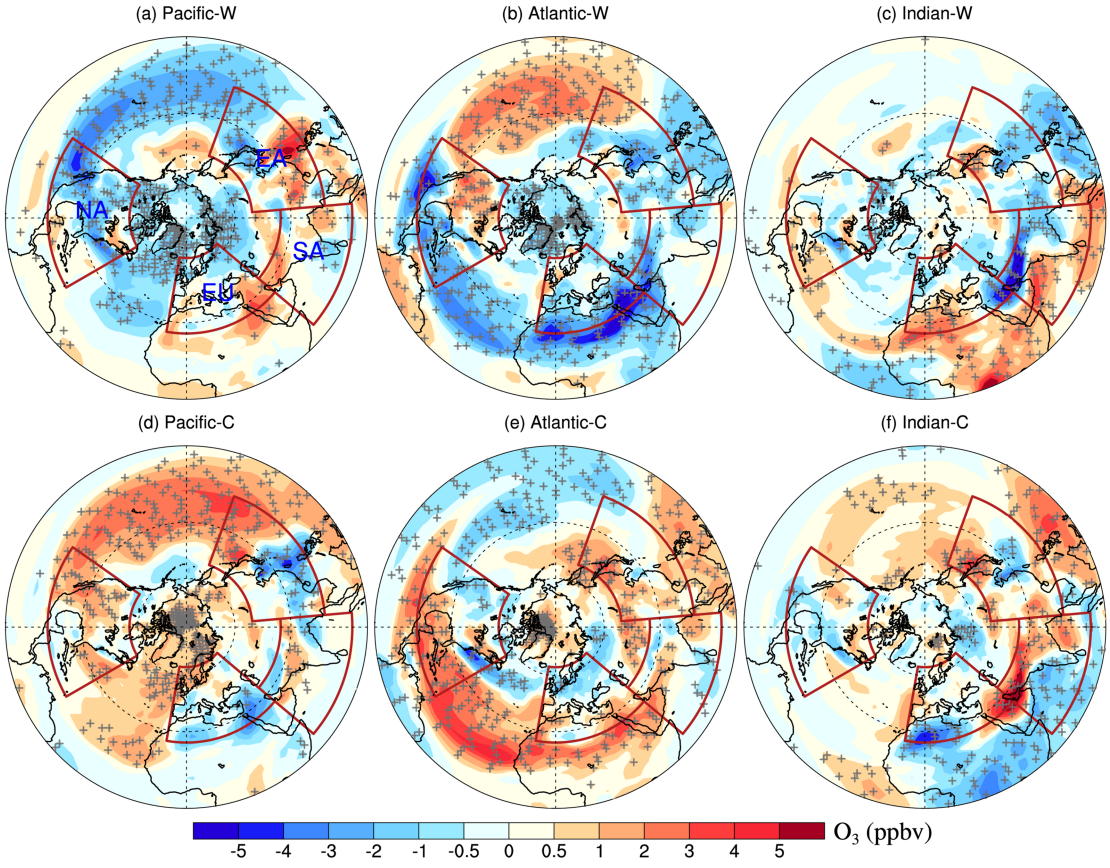

870

871 **Figure 1.** Changes in the summertime (June-August) surface O_3 concentrations (ppbv)
872 in the Northern Hemisphere induced by 1ºC warming (top) and 1°C cooling (bottom)
873 in the North Pacific Ocean (left), North Atlantic Ocean (center), and North Indian
874 Ocean (right) relative to the CTRL. The four major regions of interest (i.e., NA (15°N–
875 55°N; 60°W–125°W), EU (25°N–65°N; 10°W-50 °E), EA (15°N–50°N; 95°E–160 °E)
876 and SA (5°N–35°N; 50°E–95°E)) are marked with red polygons. The + symbols denote
877 areas where results are significant at the 0.05 level, evaluated by Student's t-test using
878 20 years of data (plots using the Mercator projection are shown in Figure S2 in the
879 supplementary material).

880

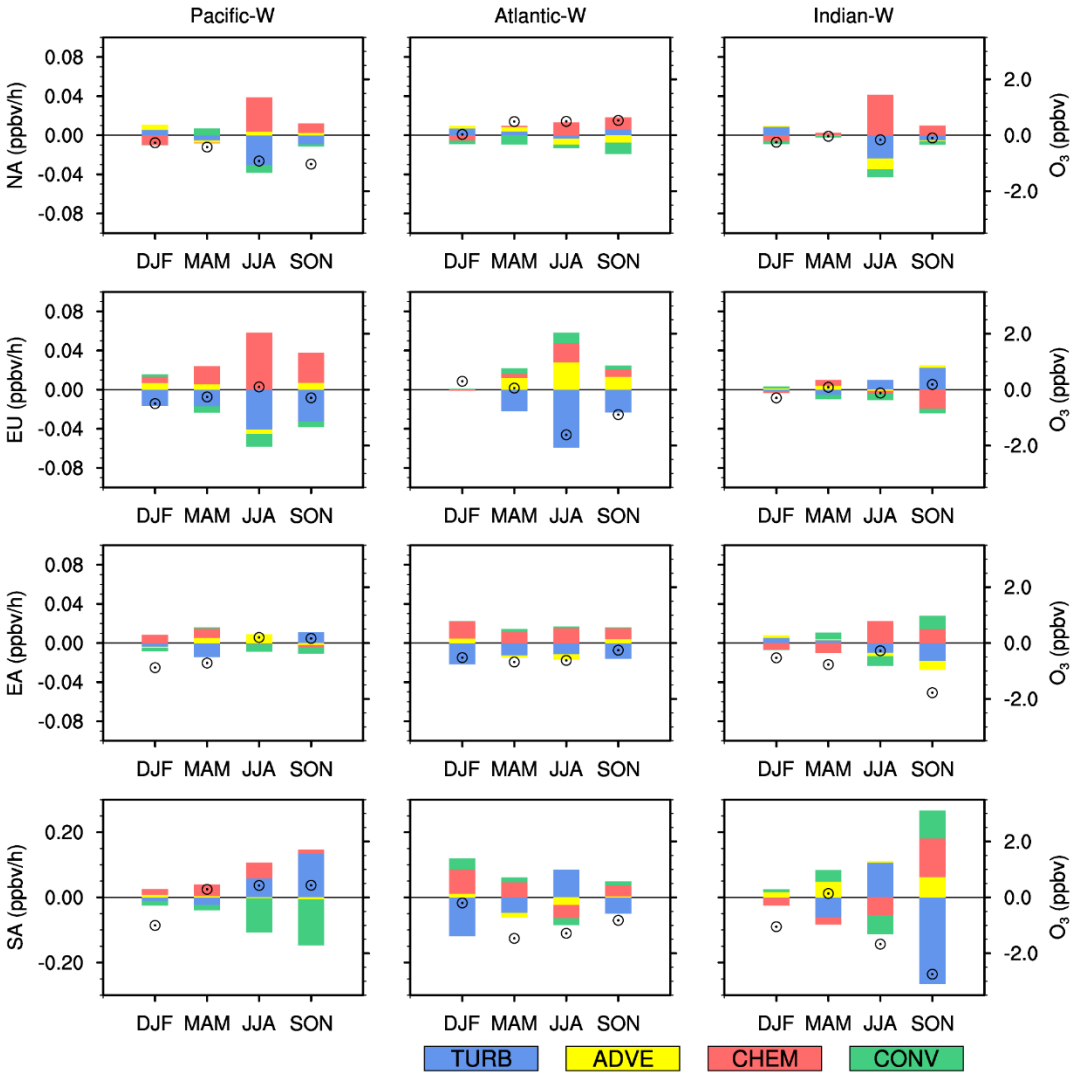

881

882 **Figure 2.** Seasonally averaged changes in the IPR contributions (bars, ppbv/h, left scale)
883 and surface O_3 concentrations (hollow circles, ppbv, right scale) for Pacific-W (left),
884 Atlantic-W (middle) and Indian-W (right) relative to the CTRL. Values are regionally
885 averaged over NA (first row), EU (second row), EA (third row) and SA (last row).
886 TURB is defined as the sum of VDIF and DRYD. CONV is the sum of DEEP and
887 SHAL. IPR contributions from the four processes (i.e., TURB, ADVE, CHEM and
888 CONV) are represented by different colors. A more detailed IPR result is shown in
889 Figure S10 in the supplementary material.

890

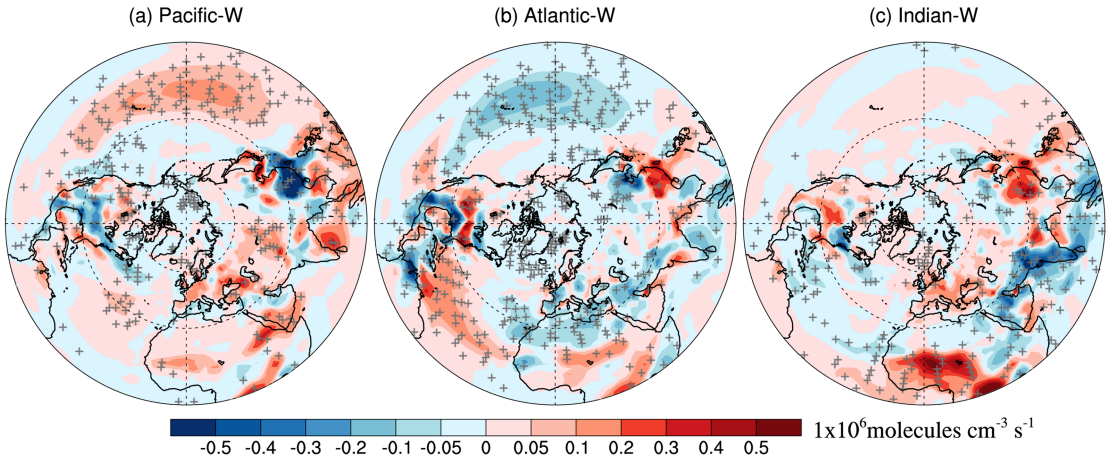

891

892 **Figure 3**. Perturbations of the surface net O_3 production rate ($1x10^6$ molecules cm^{-3} s^{-1}) for (a) Pacific-W, (b) Atlantic-W, and (c) Indian-W relative to the CTRL in the boreal
894 summer. The + symbols denote areas where the results are significant at the 0.05 level,
895 evaluated by Student's t-test using 20 years of data (plots using the Mercator projection
896 are shown in Figure S14 in the supplementary material).

897

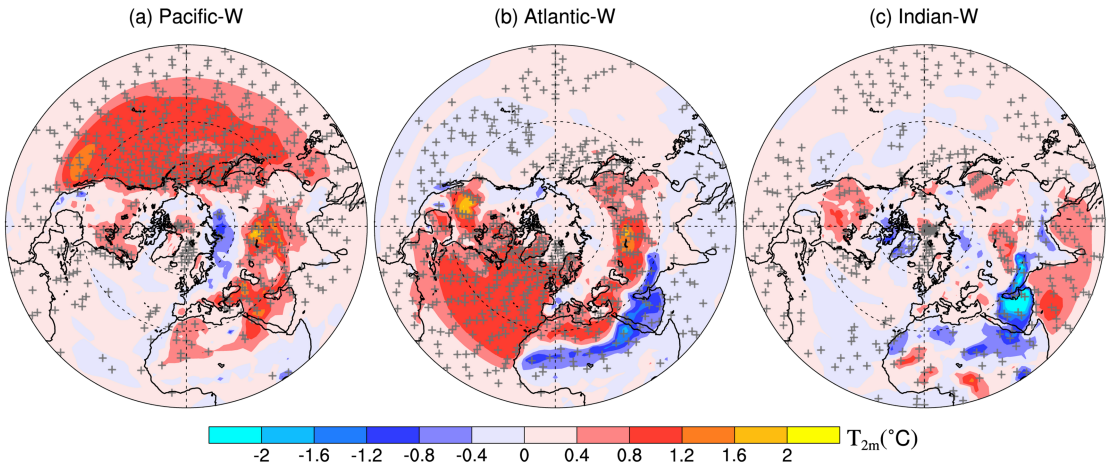

898

899 **Figure 4**. Changes in the surface air temperature (ºC) for (a) Pacific-W, (b) Atlantic-W,
900 and (c) Indian-W relative to CTRL in the Northern Hemisphere in the boreal summer.
901 The + symbols denote areas where the results are significant at the 0.05 level, evaluated
902 by Student's t-test using 20 years of data (plots using the Mercator projection are shown
903 in Figure S15 in the supplementary material).

904

905

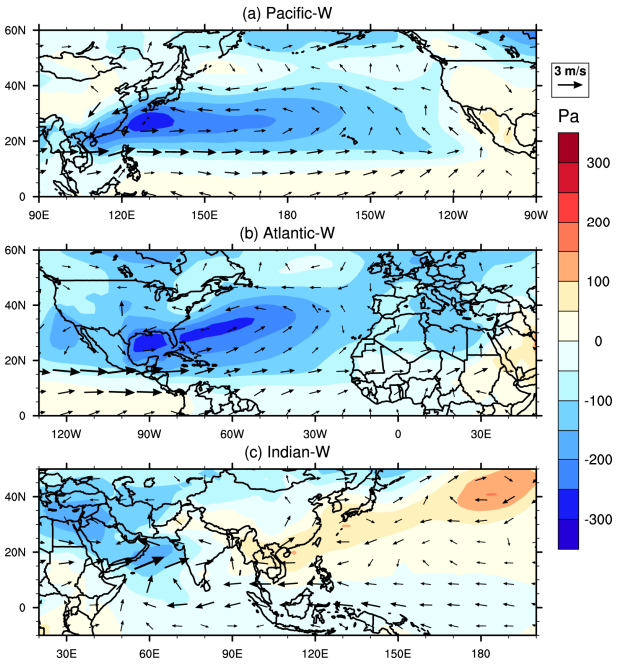

Figure 5. Changes in the surface pressure (color contours, Pa) and 850-hPa wind (arrows, m s^{-1}) for (a) Pacific-W, (b) Atlantic-W, and (c) Indian-W relative to the CTRL in the boreal summer.

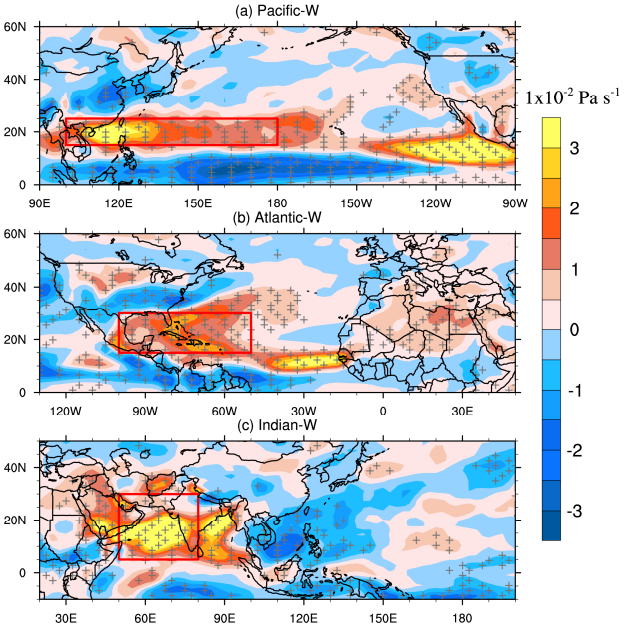

Figure 6. Spatial pattern of vertical velocity changes at 500 hPa (color contours, 1x10^{-2} Pa s^{-1}) for (a) Pacific-W, (b) Atlantic-W, and (c) Indian-W relative to the CTRL in the boreal summer. Positive values indicate upward motion. Red polygons denote the regions where the surface pressure responses to SST anomalies are significant (see

Figure 5 a-c). The + symbols indicate areas where the results are significant at the 0.05 level, evaluated by Student's t-test using 20 years of data.

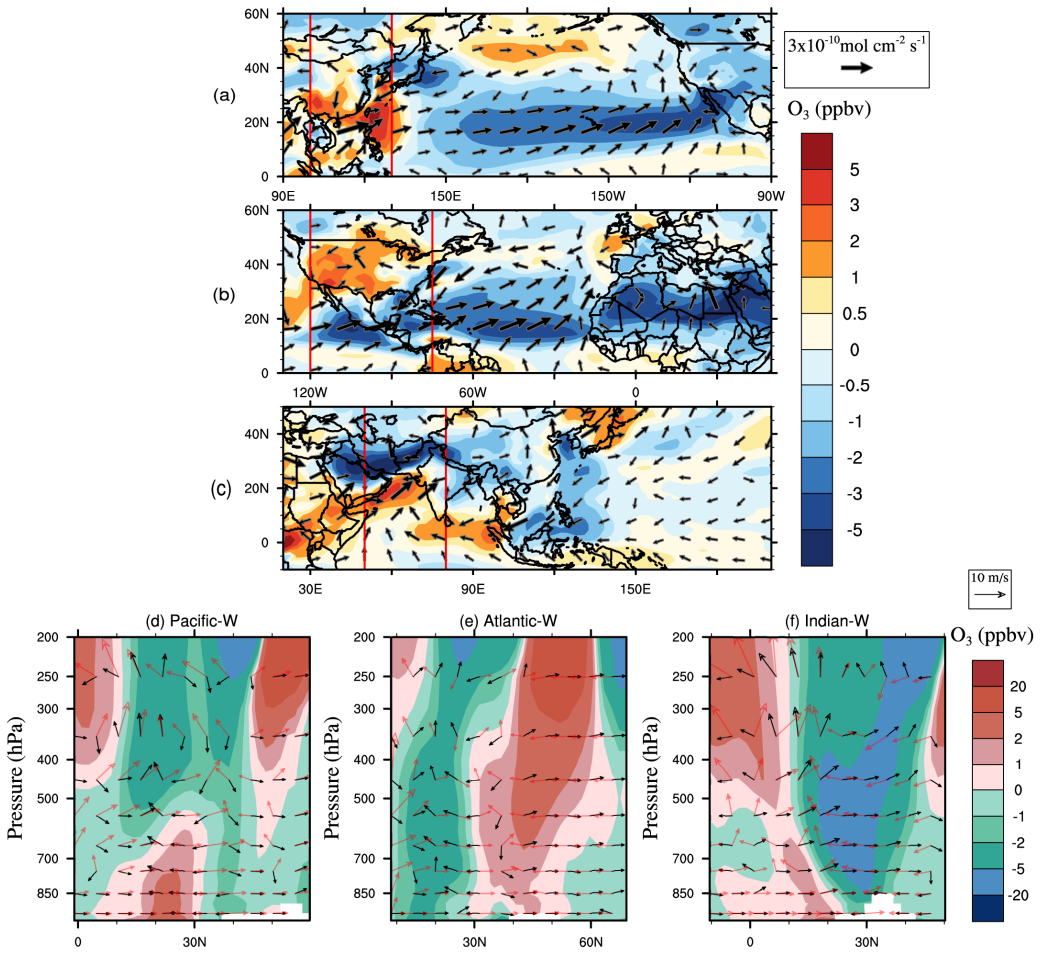

Figure 7. Top three rows: Changes in O_3 concentrations (color contours, ppbv) and horizontal fluxes (arrows, mol cm^{-2} s^{-1}) at the surface level for (a) Pacific-W, (b) Atlantic-W, (c) Indian-W relative to the CTRL in the boreal summer. Last row: zonal average of the tropospheric O_3 changes (color contours, ppbv), wind fluxes in CTRL (red arrows, m s^{-1}) and the wind flux perturbation (black arrows, m s^{-1}) in (d) Pacific-W, (e) Atlantic-W, (f) Indian-W relative to the CTRL in the boreal summer. The red rectangles in (a), (b) and (c) denote the longitudinal range used for the zonal averages in (d), (e) and (f), respectively. The vertical wind velocity is amplified 1000 times to make it comparable to the horizontal wind velocity.

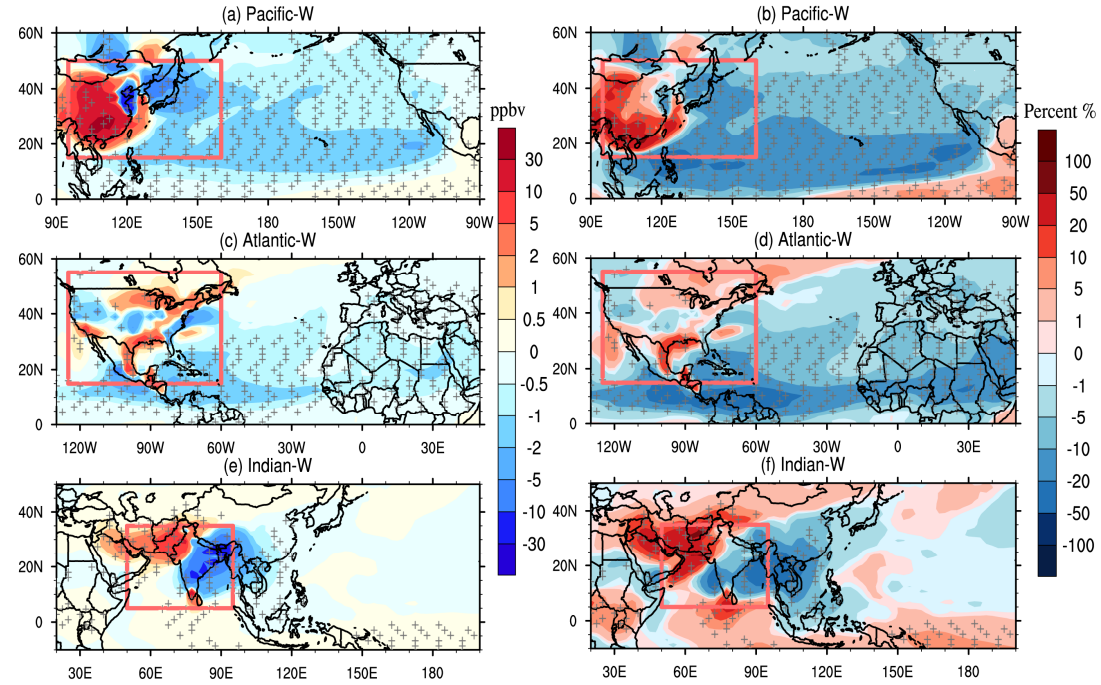

Figure 8. Left-hand panel: Difference in the surface concentration (ppbv) of a CO-like tracer emitted from (a) East Asia for Pacific-W, (c) North America for Atlantic-W and (e) the South Asia for Indian-W relative to the CTRL in the boreal summer. Right-hand panel: The percentage changes in the surface concentration of a CO-like tracer emitted from (b) East Asia for Pacific-W, (d) North America for Atlantic-W and (f) South Asia for Indian-W relative to the CTRL in the boreal summer. Red polygons denote the region where the CO-like tracer is emitted from. The + symbol denotes areas where the results are significant at the 0.05 level, evaluated by Student's t-test using 20 years of data.

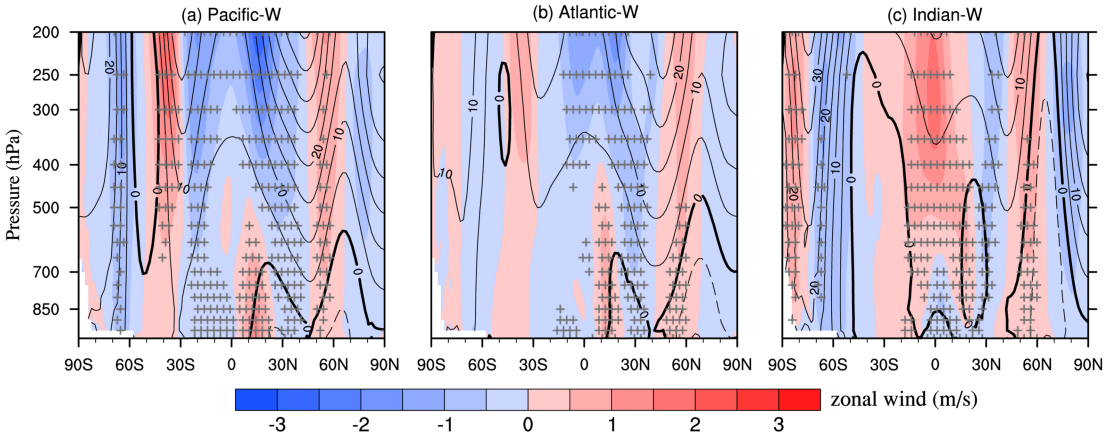

Figure 9. Zonally averaged changes in zonal wind (color contour, m/s) and geopotential

944 height (contour, m) for (a) Pacific-W, (b) Atlantic-W and (c) Indian-W relative to the
945 CTRL in the boreal summer. Black solid and dashed lines in the contours indicate
946 positive and negative geopotential height anomalies, respectively (contour interval: 5
947 m). The + symbol denotes areas where the zonal wind changes are significant at the
948 0.05 level, evaluated by Student's t-test using 20 years of data.